

Polarized Absorption Spectra of Green Fluorescent Protein Single Crystals: Transition Dipole Moment Directions[†]

Federico I. Rosell and Steven G. Boxer*

Department of Chemistry Stanford University Stanford, California 94305-5080

Received August 15, 2002; Revised Manuscript Received November 12, 2002

ABSTRACT: Polarized absorption spectra of orthorhombic crystals of wild-type green fluorescent protein (GFP) were measured between 350 and 520 nm to obtain information on the directions of the electronic transition dipole moments (\vec{m}) of the chromophore relative to the molecular axes. The transition dipole moment orientation is a basic spectroscopic parameter of relevance to biologists when interpreting Förster-type fluorescence resonance energy transfer data and for comparing absorbance and fluorescence spectra of GFP with quantum chemical calculations. Maximal extinction was obtained throughout the spectrum when the polarization direction of the electric vector of incident light was parallel to the *c*-axis of the crystal. The transition dipole moments were assumed to be parallel to the plane of the chromophore. With this assumption and the measured dichroic ratios in the crystals, the transition dipole moments associated with the neutral ($\lambda_{\text{max}} = 398$ nm) and anionic ($\lambda_{\text{max}} = 478$ nm) forms of the chromophore were found to subtend angles of $\sim 26^\circ$ and 13° (counterclockwise), respectively, with the vector that joins the phenolic and imidazolinone oxygen atoms of the chromophore.

The unprecedented popularity of the green fluorescent protein from the jellyfish *Aequorea victoria* stems from its endogenous cofactor, a *p*-hydroxybenzylideneimidazolinone group (Figure 1a; 1) that forms spontaneously as part of the protein folding process when the backbone of residues Ser⁶⁵–Tyr⁶⁶–Gly⁶⁷ cyclizes and dehydrates (2, 3). After a further oxidation step, the resulting extended aromatic chromophore interacts strongly with neighboring residues within the 11-stranded β -barrel can (Figure 1b; 4, 5) and exhibits intense fluorescence ($\Phi \sim 0.79$; 6). Perturbation of the chromophore constitution or of its immediate environment through the mutagenesis of key residues yields protein variants with altered spectroscopic and chemical properties (7). These characteristics have been exploited widely in conjunction with constantly evolving optical microscopy techniques to investigate biological processes such as protein expression, cell trafficking, localization, and function. In addition, GFP¹ variants have been engineered to act as biosensors of intracellular pH (e.g., ref 8), viscosity, local ion concentrations (e.g., ref 9), and redox potential (10). Because labeling the target system is achieved genetically even before protein expression and because in many of these protein chimeras the attached GFP does not appear to affect the properties of the target, the versatility of GFPs as imaging tools is unique.

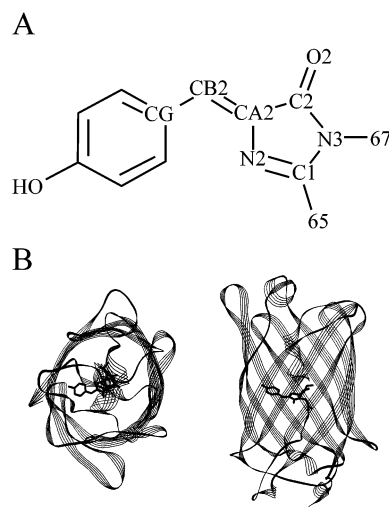


FIGURE 1: (a) Chemical structure of the *p*-hydroxybenzylidene-imidazolinone group that is the fluorescent chromophore in the green fluorescent protein from *Aequorea victoria*. 65 and 67 represent two of the three contiguous residues in the amino acid sequence from which the imidazolinone ring forms (Ser⁶⁵–Tyr⁶⁶–Gly⁶⁷, respectively). Selected atoms are labeled according to the nomenclature used in the crystal coordinate data file 1EMB (29) “Clockwise” in the text refers to rotations based on the orientation of the chromophore as shown here. (b) Two views of a ribbon representation of the green fluorescent protein from *Aequorea victoria* showing the chromophore within the interior of the eleven-stranded β -sheet cylinder.

[†] This work was supported by the National Institutes of Health under Grant GM27738.

* To whom correspondence should be addressed. E-mail: sboxer@stanford.edu. Phone: (650)723-4482. Fax: (650)723-4817.

¹ Abbreviations: GFP, green fluorescent protein; HEPES, *N*-(2-Hydroxyethyl)piperazine-*N'*-(2-ethanesulfonic acid); Ni-NTA, nickel nitriloacetic acid; PMSF, phenylmethylsulfonyl fluoride; OD_{||c} and OD_{⊥c} are the optical densities of a crystal at specific wavelengths when light is polarized parallel or perpendicular to the crystallographic *c*-axis, respectively; E_{||c} and E_{⊥c} refers to spectra measured with the electric field of incident light polarized parallel or perpendicular to the *c*-axis.

Under native conditions, the chromophore in wild-type GFP exists primarily in one of two states that are in a pH-linked equilibrium. The A-state, associated with the neutral form of the chromophore, is characterized by a broad absorbance band centered at 398 nm that remains largely featureless on freezing down to 77 K (11). With increasing pH, deprotonation of the chromophore is accompanied by

the rearrangement of neighboring residues within the chromophore cavity (12). The resulting B-state absorbs at 478 nm and, unlike the neutral chromophore, exhibits a prominent Stark effect as well as resolved vibronic structure at cryogenic temperatures (13). At room temperature, excitation of either the A- or B-states results in fluorescence at wavelengths longer than 500 nm. Short-lived (picosecond) fluorescence can be detected between 420 and 470 nm upon excitation of the A-band. However, a picosecond excited-state proton-transfer process competes with direct fluorescence from A* by converting this species into an intermediate I* that resembles B* electronically and fluoresces above 500 nm (11).

The direction of the transition dipole moment \vec{m} is the cornerstone of any spectroscopic application for which the interpretation of results depends on geometric factors. In Förster-type fluorescence resonance energy transfer (FRET) experiments, for example, the rate depends strongly on the projection of the emitting transition dipole moment onto that of the absorbing dipole (the κ^2 factor; 14). The high fluorescence anisotropy exhibited on excitation of either the A- or the B-states, under conditions where protein rotation are minimized ($r = 0.22-0.38$; 480–600 nm; 11) show that the absorption and emission transition moments of both protonation states are within a few degrees from one another. To translate observed FRET or other orientation-dependent measurements into molecular terms, however, the directions of the transition dipole moments with respect to the molecular axes of the protein must be mapped. This spectroscopic parameter has been determined successfully for a number of biologically relevant chromophores by measuring the polarized absorption spectra of single crystals (15–19). In the case of proteins where the chromophore of interest is encapsulated by the polypeptide (20–25), the protein matrix both provides a fixed orientation and maintains a considerable distance between chromophores so that interchromophore interactions have a minimal effect on the electronic absorption. This ideal situation is sometimes referred to as an “oriented gas” of chromophores. In the following we report the results of measurements on orthorhombic crystals of wild-type GFP to establish the orientation of \vec{m} with respect to the molecular axes of the protein. A preliminary account of these results was presented at a recent conference (26). While this work was being prepared for publication, a paper appeared on the fluorescence polarization of GFP single crystals (27). The relationship between fluorescence and absorption experiments is discussed.

EXPERIMENTAL PROCEDURES

Protein Preparation and Crystallization. Wild-type GFP was expressed essentially as described elsewhere (28) with *E. coli* BL21(DE3)pLys and the plasmid pRSET_b-GFP. α -Chymotrypsin which had been incubated for 1 h at room temperature in 20 mM HEPES buffer, pH 8.0, was added (1:25 w/w; Sigma) to cleave the N-terminal poly-His purification tag. After overnight incubation at room temperature, the protease was deactivated by addition of PMSF to 100 μ M. The resulting protein mixture was filtered through a fresh Ni-NTA agarose chromatography column, and the unretained GFP was collected for further purification by anion exchange chromatography (Toyopearl DEAE-650S). The fractions of the wild-type protein exhibiting an absor-

bance ratio (A_{397}/A_{280}) ≥ 0.8 were pooled, concentrated and exchanged into 10 mM Tris buffer, pH 8.0 for crystallization. Protein concentrations were estimated at each step based on an extinction coefficient of 26 mM⁻¹ cm⁻¹ at 280 nm.

Crystallization of the protein (~ 15 mg/mL) was achieved with a few modifications to the protocol of Brejc et al. (29). The principal differences are that crystallization was induced initially by triturating a crystal of the Ser65Thr variant to microseed the crystallization, sodium azide was excluded from the mother liquor solution, and the crystals were obtained by hanging drop vapor diffusion. After 2–3 weeks, small, needlelike crystals were collected, washed with 10 mM Tris buffer pH 8.0, and incubated overnight at room temperature in 4–5 volumes of buffer. The protein that dissolved during this incubation period was collected and used in a second round of crystallization. This time, microseeding was either not performed or achieved with fragments of a crystal of the wild-type protein. The mixtures were incubated at room temperature until crystals large enough for spectrophotometric analysis under a microscope could be collected.

Crystals were washed in fresh mother liquor (20% PEG 4000, 50 mM potassium phosphate buffer, pH 3.8) and transferred to a 50 μ L buffer droplet (1:1 mixture of mother liquor and 10 mM Tris buffer, pH 8.0) on a clean quartz microscope slide. Before sealing the samples, crystals were manipulated to lie flat on this slide. Clean 2 \times 2 \times 0.075 cm quartz plates were used as coverslips, and seals were achieved with 120 μ m thick, double-sided, self-adhesive spacers (Molecular Probes). Crystals were selected for examination if they met a list of criteria intended to minimize optical distortions and to ensure that the samples under scrutiny were monocrystalline. First, the edges along the length of the crystal were in focus under the microscope, and the surface appeared blemish/crack free. Crystals near air bubbles were either moved to avoid interference from geometric stray light arising from a meniscus, or they were not used for measurements. Finally, the crystals between crossed polarizers exhibited uniform fluorescence and uniform color changes when turning the polarization of white light illumination incident normal to the crystal.

Absorption Dichroism Measurements. Absorption of plane polarized light by single crystals of wild-type GFP was measured with a Zeiss Photomicroscope II fitted with a photodiode detector (EG&E, HUV-1100BQ), the output of which was fed into a lock-in amplifier (SR850, Stanford Research Systems). Light from a 300 W xenon arc lamp was dispersed with a single grating monochromator (Spex Model 1681, $f = 0.22$ m, 1.25–2.50 mm slits, 3.7 nm/mm dispersion at 500 nm, 0.25 nm resolution), chopped (400 Hz), focused, and collimated into the microscope with quartz lenses. The monochromator was calibrated with the 632.8 nm line of a HeNe laser and checked frequently with sharp band-pass filters. The light was polarized with a Glan-Thompson polarizer, masked with an adjustable, rectangular slit to limit the field of illumination to the area encompassed by the crystal under scrutiny, and focused on the crystal with a 10x substage objective. The transmitted light was collected with either a 16 \times or a 20 \times objective lens, and any fluorescence ($\lambda > 500$ nm) was rejected with a short-pass filter that was placed immediately in front of the detector. Geometric stray light (18) encountered with this setup was estimated to be

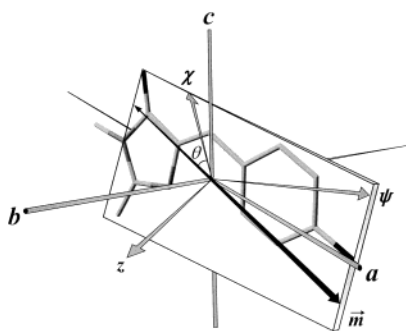


FIGURE 2: Coordinate axes systems that relate the orientation of a transition dipole moment (\vec{m}) of the GFP chromophore as defined by the plane of the benzylideneimidazolinone group (χ , ψ , z) to the crystallographic axes (a , b , c). χ and ψ are in the plane of the chromophore that is illustrated as a rectangle. χ is also the intersection of the ac and the chromophore planes. θ represents the angle between χ and the transition dipole moment in the plane of the chromophore.

of the order of the dark current of the detector ($\sim 5 \mu\text{V}$, chopped) and therefore not significant except at very high optical densities. The intensity of the transmitted light as a function of wavelength (with light polarized at $\mathbf{E}_{\parallel c}$ and $\mathbf{E}_{\perp c}$) or polarization angle (monitored at 410 and 470 or 475 nm) was measured and transformed to absorbance using blanks collected by sliding the sample to a clear region immediately beside the crystal. This transformation also compensated for the small polarization bias of the microspectrophotometer. An experimental uncertainty of $\pm 2^\circ$ is associated with the angle of polarization. The maximum absorbance that could be measured with confidence (< 3) was determined from a calibration of the setup with respect to a Perkin-Elmer Spectrophotometer, Model Lambda12, with a combination of neutral density filters that were placed in the light path (410 nm) immediately in front of the microscope.

Trigonometric Analysis. The analysis of the absorption anisotropy of a crystal of P_{212121} symmetry was described in an earlier polarization spectroscopy study conducted on single crystals of a chlorophyllide–apomyoglobin complex (24). A key simplifying assumption is that all \vec{m} lie in the plane of the chromophore. Because of this assumption, it is not necessary to measure the absorption dichroism along all three principal dichroic axes of the crystal. This is often not possible, as in the present case, because the crystals tend to grow as needles that are difficult to align with the long axis parallel to the incident beam, or the dimensions limit light throughput either because of small cross-sectional area or because of a long path length.

An orthogonal axis system is defined by the axes χ , ψ , and ζ so that the $\chi\psi$ plane is parallel with the chromophore plane (Figure 2). The χ -axis is chosen to lie parallel to the ac plane of the crystal, and it acts as the reference axis from which the angle to \vec{m} is traced. In this coordinate system, the transition dipole moment can be described in terms of its components along these axes according to eq 1:

$$\vec{m} = \hat{\chi} \cos \theta + \hat{\psi} \sin \theta + \hat{z} \sin \phi \quad (1)$$

where θ and ϕ are the angles between \vec{m} and the χ and z axes, respectively, and the carats denote unit vectors. Because, as mentioned above, the out-of-plane component of the transition moment (i.e., the z -component) is assumed to be nonexistent, the third term is dropped, and \vec{m} is defined

primarily in terms of its θ terms. Furthermore, the absorption dichroism observed with light incident normal to the ij plane of the crystal (where i and $j \equiv a, b, \text{ or } c$ crystallographic axes) is proportional to the squares of the projections of the transition moment onto the crystallographic axes:

$$\frac{\text{OD}_i}{\text{OD}_j} = \frac{(\hat{e}_i \cdot \vec{m})^2}{(\hat{e}_j \cdot \vec{m})^2} = \left[\frac{(\hat{e}_i \cdot \hat{\chi}) \cos \theta + (\hat{e}_i \cdot \hat{\psi}) \sin \theta}{(\hat{e}_j \cdot \hat{\chi}) \cos \theta + (\hat{e}_j \cdot \hat{\psi}) \sin \theta} \right]^2 \quad (2)$$

Note that all four chromophores in the unit cell will exhibit the same dichroism by virtue of the space group symmetry. Therefore, selecting the chromophore for which the directional cosines are positive, eq 2 can be reformulated in terms of the crystallographic axes using the transformation operations shown below:

$$\begin{aligned} \hat{e}_a \cdot \hat{\chi} &= \frac{z_b}{\sqrt{\alpha}} & \hat{e}_b \cdot \hat{\chi} &= -\frac{z_a}{\sqrt{\alpha}} & \hat{e}_c \cdot \hat{\chi} &= 0 \\ \hat{e}_a \cdot \hat{\psi} &= \frac{z_a z_c}{\sqrt{\alpha}} & \hat{e}_b \cdot \hat{\psi} &= -\frac{z_b z_c}{\sqrt{\alpha}} & \hat{e}_c \cdot \hat{\psi} &= -\sqrt{\alpha} \end{aligned} \quad (3)$$

where $\alpha = 1 - z_c^2$. The directional cosines, $|z_a| = 0.461$, $|z_b| = 0.880$, and $|z_c| = 0.114$, were determined from the published crystal structure of wild-type GFP (Protein Data Bank code 1EMB; (29); see Supporting Information). In this model, the planes of the four chromophore in each unit cell are nearly perpendicular to the ab crystal plane, but they are inclined approximately 25 and 65° relative to the ac and bc planes, respectively. Consequently, the polarization ratios measured with light incident normal to the ac or bc faces of the crystal are expected to be very similar.

The dependence of the measured polarization ratios as a function of the angle θ are given by²

$$\frac{\text{OD}_c}{\text{OD}_a} = \left[\frac{\alpha}{z_b \cot \theta + z_a z_c} \right]^2 \quad (4)$$

$$\frac{\text{OD}_c}{\text{OD}_b} = \left[\frac{\alpha}{z_a \cot \theta - z_b z_c} \right]^2 \quad (5)$$

$$\frac{\text{OD}_a}{\text{OD}_b} = \frac{z_b^2 \cot \theta + z_a^2 z_b^2 \tan \theta + 2z_a z_b z_c}{z_a^2 \cot \theta + z_b^2 z_c^2 \tan \theta - 2z_a z_b z_c} \quad (6)$$

Thus, recalling that θ in this case is the angle between the transition moment and the reference axis χ , a plot of eqs 4 and 5 (Figure 3) illustrates the magnitude of the dichroic ratios expected as a function of this angle.

RESULTS

GFP Crystals. Crystallization of wild-type GFP under the conditions used here yields protein crystals of P_{212121} symmetry with four monomeric chains per unit cell. Diffraction data were not collected; however, the dimensions (~ 0.03 –

² Equation 6 is included in the text to correct a typographical error in ref 24.

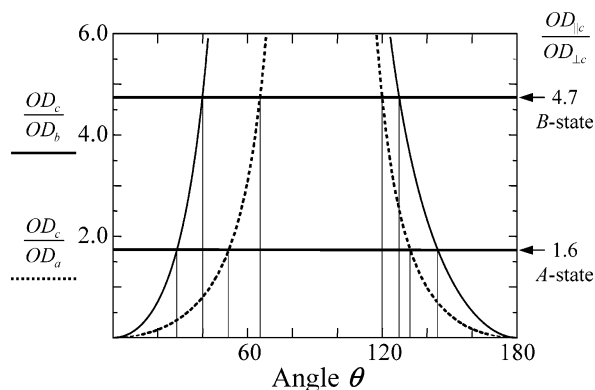


FIGURE 3: Polarization ratios derived from eqs 4 and 5 as a function of the angle θ between the transition dipole moment of the chromophore in wild-type GFP and the reference axis χ when viewed with light incident to the ac (—) or bc (---) crystallographic planes. The values cited in the column on the right side of the graph are the averaged linear dichroism values determined at 410 and 470 nm, for the A- and B-states, respectively (see Figures 4 and 5).

0.08 mm to a side and 0.3 mm long) and morphology of these crystals (i.e., hexagonal needles) are comparable to those reported elsewhere for the orthorhombic form (4, 29).

The crystals used for spectrophotometric investigation were of varied thickness and widths so that a range of optical densities (1.8–3.8 for A_{410} and 0.4–2.2 for A_{470}) was sampled. Smaller crystals were rejected because of problems inherent in masking an area large enough for reliable transmittance measurements while avoiding geometric stray light. At the opposite extreme, measuring the high optical densities associated with larger crystals was also unreliable because of the reduced transmittance. Therefore, spectral regions with absorbance values greater than ~ 3 were considered in the analyses only for qualitative purposes. Next, fluorescence from the crystal, most evident when the sample was placed between crossed polarizers, was interpreted as an indication that the protein retains the native fold in the crystal. Because this fluorescence interfered significantly with the absorbance measurements, a short-pass filter (transmittance < 490 nm) was included immediately before the detector to avoid artificially higher apparent transmission readings arising from fluorescence. With this arrangement, essentially no light above background could be detected over the wavelength range of interest indicating that crystal birefringence was not significant. In addition to exhibiting fluorescence, the protein in the crystals appeared to be stable during the course of a day's measurements. Little or no photoconversion from the A- to B-states of the protein was evident from the absorption even after prolonged (days) irradiation at 410 nm. However, protonation of an increasing number of molecules did appear to take place over the course of a few days in response to the pH of the crystal mounting solution (pH ~ 3.9). In this environment, the crystallized protein presumably titrated slowly so that the A-state became more populated with time at the expense of the B-state.

Absorbance Polarization Measurements. Figure 4 shows the absorbance of wild-type GFP crystals at 410 and 475 nm as a function of the polarization angle (θ_p) fitted to the relation expected for an orthorhombic crystal as derived by Simpson and co-workers (17, 30):

$$OD(\theta_p) = -\log[10^{-OD_{\parallel c}} \cos^2 \theta_p + 10^{-OD_{\perp c}} \sin^2 \theta_p] \quad (7)$$

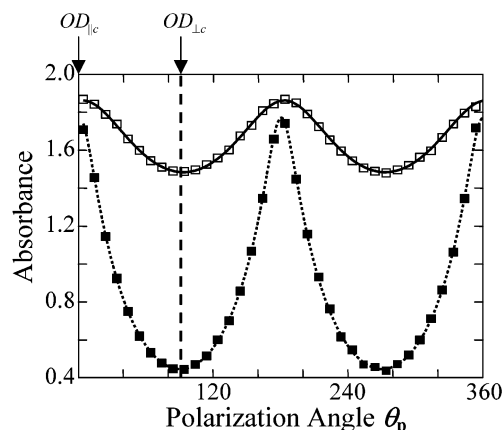


FIGURE 4: Angular dependence of the absorption of plane-polarized light by an orthorhombic crystal of wild-type GFP (pH ~ 3.9) measured at 410 (\square) and 475 (\blacksquare) nm. θ_p refers to the angle subtended between the \mathbf{E} field of the incident plane-polarized light and the crystallographic c -axis. The curves are the results from least-squares fitting of the data to eq 7 and yield the ratios ($OD_{\parallel c}/OD_{\perp c}$) that are shown on the right side of Figure 3.

Good agreement of these data to eq 7 has been used in previous studies to assess the quality of similar dichroism measurements on single crystals (18, 24, 30). From the parameters obtained by fitting the polarization angle modulation (i.e., $OD_{\parallel c}$ and $OD_{\perp c}$), the averaged polarization ratios at 410 and 470 nm were determined to be 1.6 and 4.7, respectively.

Crystals of the Ser65Thr variant, whose chromophore is predominantly in the anionic form, also exhibit greatest extinction at 450 and 480 nm when incident light is polarized parallel to the crystallographic c -axis. The averaged polarization ratio calculated after fitting the angular dependence of the crystal absorbance to eq 7 is 3.0, in contrast to the nominally equivalent value of 4.7 determined for the wild-type protein B-state absorption. At first sight, this difference could be interpreted to stem from different orientations of \vec{m}_B (i.e., the transition dipole moment direction of the anionic form in the plane of the chromophore of this variant and of wild-type GFP). However, we note that from the directional cosines of the chromophore in the three-dimensional models of the Ser65Thr variant (1EMA (4), 1C4F, or 1EMG (12)), the plots of eqs 4 and 5 shift appreciably to compensate in some cases for the difference in polarization (see supplementary information).

The spectra of a protein crystal measured with the electric vector of incident light parallel ($\mathbf{E}_{\parallel c}$) or perpendicular ($\mathbf{E}_{\perp c}$) to the crystallographic c -axis are shown in Figure 5. The associated polarization ratio calculated as a function of wavelength (i.e., $(\mathbf{E}_{\parallel c}/\mathbf{E}_{\perp c})$) is illustrated in the inset. Of the two crystal spectra, $\mathbf{E}_{\perp c}$ resembles the solution spectrum more closely (dotted line, pH ~ 3.7). Scrutiny of these spectra reveals that in the region of the B-band, the absorption of light polarized along the c -axis (i.e., $\mathbf{E}_{\parallel c}$) is approximately 4-fold greater than when it is polarized perpendicular to this crystal axis. This high dichroism spans the wavelength region from 430 to 500 nm, while in the A-band region the absorption profiles of the crystal differ only by $\sim 20\%$. The difference in the polarization ratios observed for the neutral and anionic forms of the chromophore implies that the transition moments of the two species are not parallel to one other. From the polarization ratios and with the assumption

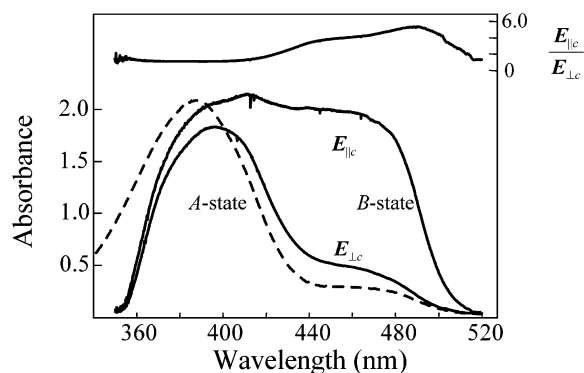


FIGURE 5: Comparison of the absorption spectra of an orthorhombic single crystal of wild-type GFP (—) measured with the electric vector (\mathbf{E}) of plane polarized light parallel (\parallel) or perpendicular (\perp) to the crystallographic c -axis. The spectrum of the protein in solution measured at pH 3.7 is shown for reference purposes, and the inset shows the wavelength dependence of the polarization ratio.

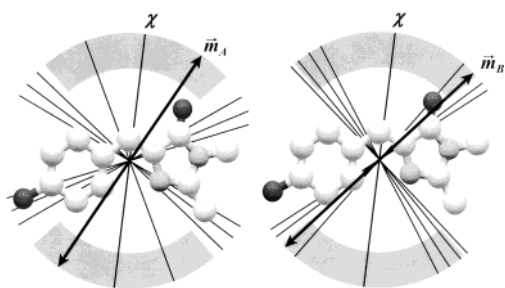


FIGURE 6: Possible orientations of the transition dipole moments \vec{m} of the p -hydroxybenzylideneimidazolinone group in the neutral (A) and anionic (B) forms of this fluorophore in wild-type GFP. These orientations represent the projections of the transition moments of each of the four units in each unit cell of the crystal onto the crystallographic axes. The projections shown as bold, double-headed arrows are the solutions selected based on the criteria and assumptions outlined in the text. The arches shown in gray delineate the maximum inclination (45°) with respect to the crystallographic c -axis that is possible for the direction of \vec{m} to yield maximal extinction along the length of the crystal. The equations of the unit vectors that express the orientations of the dipole moments in terms of the coordinate axes system defined in the Protein Data Bank (1EMB) are $\vec{m}_A = 0.55a + 0.20b - 0.81c$ and $\vec{m}_B = 0.74a + 0.22b - 0.63c$.

that both transition moments lie in the chromophore plane, a set of four projections of \vec{m} are found that satisfy eq 4 and a second set of four projections that satisfies eq 5 (Figures 3 and 6). Finally, the trigonometric analysis described in the Experimental Section yields a value for the angle θ but no information regarding the direction on the plane of the chromophore with respect to the reference axis χ . Consequently, each set of four projections is doubled to yield a total of 16 projections from which possible physical orientations of \vec{m} can be identified.

The scatter in the polarization ratios collected for different crystals introduces an uncertainty in the derived orientation of \vec{m} of $\pm 4^\circ$. Also, as illustrated by the differences found in the dichroism associated with wild-type GFP crystals and those of the Ser65Thr variant (see supplementary information), the conclusions from this analysis depend strongly on the accuracy of the chromophore coordinates. Both the protonated and deprotonated forms are present in the crystals. At the resolution of the crystal model of wild-type GFP (2.13 Å), for example, it is possible that the chromophores that

are deprotonated have a slightly different orientation than do the majority of molecules that are in the neutral state. Although Remington and co-workers do not report explicitly such heterogeneity in the chromophore coordinates as they do for a number of residues in the model 1EMB (e.g., Thr203), subtle structural differences between the two protonation states of the chromophore may contribute appreciably to the difference between the orientations of the projections of \vec{m}_A and \vec{m}_B .

DISCUSSION

Transition Dipole Moment Orientations. Analysis of the absorption polarization dichroism exhibited by orthorhombic crystals of wild-type GFP yields a number of solutions that represent the projections onto the crystallographic axes of the transition dipole moment of each of the two protonation states of the p -hydroxybenzylideneimidazolinone group (Figure 6). These solutions are illustrated for the neutral and anionic forms of the chromophore (panels A and B, respectively). To identify the orientation of these \vec{m} with respect to the molecular axes from these sets of projections, the directions must be consistent with a number of observations. First we recall from the angular dependence of the crystal absorbance (Figure 4) that maximal extinction of light throughout the spectrum is achieved with light polarized along the crystallographic c -axis. This result establishes an upper limit of 45° for the angle subtended between the projection of \vec{m} and the c -axis of the crystal. A greater angle would result in greater extinction perpendicular to c instead. Upon inspection of the relative orientation of each of the four protein chains in a unit cell of the crystal, an area was identified as illustrated in Figure 6 by the gray arches that encompasses the boundaries within which the transition dipole moments of the chromophore may reside. This condition excludes approximately half of the projections shown in the figure, the vector parallel to the long axis of the chromophore which is parallel to a line between CG2 and CA2 in Figure 1 (hitherto assumed in the literature to be the direction of the transition moment), and the orientation determined by INDO/S-CI calculations ($\sim 8^\circ$, counterclockwise, from the exocyclic double bond between CB2 and CA2 in Figure 1; 31).

Next, we note that the room-temperature fluorescence anisotropy of wild-type GFP in a 90% glycerol solution is ~ 0.38 regardless of whether the sample is excited at 397, 405, or 477 nm (data not shown). These results indicate that the absorption and fluorescence transition dipole moments of the anionic form of the chromophore (\vec{m}_B , B-state, 477 nm) are essentially coincident. Likewise, the absorption transition moment of the neutral form (\vec{m}_A , A-state, 390 nm) is nearly parallel to the emission transition moment of the excited intermediate species that forms following excited-state proton transfer of the A*-state (11). Because the electronic structure of this intermediate form of the chromophore is likely similar to that of the B-state, the orientations of the transition dipole moments \vec{m}_A and \vec{m}_B are probably very similar also. An indication that these orientations may be subtly different comes from the fluorescence anisotropy of GFP measured at 77 K (11). Under these conditions the value of r dips noticeably at ~ 490 nm from its value above 500 nm ($r \sim 0.3$) on excitation of predomi-

nantly the A-state (404 and 423 nm; fluorescence from I*). By comparison, there is no evidence of this dip when the B-state is excited directly (471 nm), thus suggesting that the orientations of the emission moments of B* and I* are not exactly the same. These observations neither reduce the number of possible orientations of \vec{m}_A and \vec{m}_B , nor do they answer the question of whether there is a protonation state-dependent structural difference in the crystal lattice, but they link the two transition moments to reside in a similar orientation. Therefore, the polarization ratios determined for the A- and B-band regions for each crystal must satisfy concurrently the two criteria listed above.

Finally, we consider the Stark effect on the absorption spectrum of GFP. Publitz et al. observed a change in dipole moment ($|\Delta\mu|$) of 6.8 D and an angle ζ_A of 21° between \vec{m}_B and $\Delta\vec{\mu}$ for the B-state of wild-type GFP (13). The authors interpreted these results on the basis of the probable identification of the oxygen atoms of the phenolic and imidazolinone rings as sites of charge density transfer upon excitation. These atoms, separated by $\sim 9 \text{ \AA}$, are related through resonance when the chromophore is deprotonated such that subtle shifts in charge density between these sites upon excitation can elicit a significant difference in the dipole moment. The large $|\Delta\mu|$ observed suggests that this assessment is correct and thus implies that the transition dipole moment lies $\sim 21^\circ$ with respect to the vector that joins these two oxygen atoms.

From the potential orientations of \vec{m} shown within the gray arches in Figure 6, only one set of projections satisfies the criteria listed above. The probable orientation of \vec{m}_A and \vec{m}_B are illustrated in the figure as bold, double-headed arrows clockwise $\sim 27^\circ$ and 40° , respectively, from the reference axis χ defined in the Experimental Section. The solution identified as \vec{m}_B is oriented $\sim 16^\circ$ from the line between the phenolic and imidazolinone oxygen atoms in close agreement with the criterion defined based on the Stark spectroscopy results. As determined from the high fluorescence anisotropies of GFP and based on the similarities of the electronic structures of the B- and I-states, the projection corresponding to \vec{m}_A is therefore similar, subtending a 13° angle with \vec{m}_B as shown in panel A of the same Figure.

Single-Crystal Fluorescence Anisotropy. While this manuscript was in preparation, a paper was published documenting a high degree of polarization of the fluorescence from GFP single crystals (27). The analysis of the emission polarization presented by Inoué and co-workers is not related to the analysis of absorption polarization reported here. At issue is whether the fluorescence from the crystal reflects the spectroscopic properties of isolated GFP chromophores, or whether it is influenced strongly by the energy transfer that can occur between GFP chromophores in the closely packed crystal lattice. By working with a protein host matrix that absorbs at much higher energy than the chromophore whose polarization properties are under investigation, one achieves the “oriented gas” condition for a polarized absorption experiment. In the case of the GFP crystals presented here, this condition is satisfied because the closest distance between GFP chromophores in the orthorhombic crystal is 37.5 \AA center-to-center, or 31.6 \AA closest approach. At this distance, interchromophore exciton interactions are much smaller than the inhomogeneous line width or vibronic spacing of the chromophore, so that the chromophores are

isolated from each other. The analysis of the absorption polarization data presented above is predicated upon this condition being true, and the excellent fit of the polarization data in Figure 4 to the theoretical curve of eq 7 demonstrates that the analysis is valid. In the fluorescence polarization experiment, Inoué and co-workers noted a very high emission anisotropy in the crystal, and the emission obeyed a different relationship than eq 7. The relationship of Simpson and co-workers (eq 7) should apply for fluorescence polarization as for absorption so long as the chromophores are isolated.

We believe that the difficulty in this analysis results from the assumption of the oriented gas condition applied to fluorescence from these crystals. Each GFP chromophore in the $P_{2,2,2}$ lattice has many other chromophores (at least 6) within the Förster critical transfer radius ($R_0 \approx 46.5 \text{ \AA}$ (32)). R_0 is the distance at which 50% of excited states transfer energy nonradiatively by FRET, and the other half emits a photon. The efficiency of FRET also depends on the spectral overlap and on κ^2 , a measure of the projection of the transition dipole moment of the emitting state (the donor) on that of the absorbing state (acceptor) and on the vector that connects the centers of these participants. Because energy transfer in pure GFP crystals is degenerate, the spectral overlap is fixed by the small Stokes shift of the emission while κ^2 is different for different combinations of GFP pairs in the crystal. With the absorption polarization data described above and the known crystal lattice, one could calculate the many pathways available for efficient energy transfer between chromophores for each initially excited site. Fluorescence will often originate from a different chromophore than the one which was excited originally (though excitations may re-visit the site of original excitation), and more significantly, it will be characterized with a different polarization. The “oriented gas” condition of isolated chromophores does not apply to fluorescence from these crystals, and consequently, one cannot use this approximation to analyze the data. Furthermore, one expects averaging of the effective emission polarization direction around symmetry axes of the crystal (not simply projections, as in absorption, but averaging due to FRET). In fact, Inoué and co-workers observed a very high level of polarization that would be inconsistent with the absorption dichroism if the emission were for isolated chromophores. Because the emission is not associated with any individual chromophore, no direct information can be obtained about the direction of the isolated transition moments. This issue could be circumvented by cocrystallizing the Ser65Thr variant of GFP as a guest with another protein host that absorbs at higher energy (for example BFP (Tyr66His) or with α -lactose monohydrate which was recently shown to serve as a crystalline host for GFP (31)).

ACKNOWLEDGMENT

The authors would like to thank Prof. Rebekka Wachter, Dr. George Hanson, and Mr. Daniel Yarbrough for providing useful information regarding the crystallization of GFP. The help of Mr. Thomas Treynor is also greatly appreciated. F.I.R. gratefully acknowledges a postdoctoral fellowship from the Natural Sciences and Engineering Research Council of Canada.

SUPPORTING INFORMATION AVAILABLE

Chromophore orientations in the crystal and comparison of the dichroism of wild-type GFP and Ser65Thr variant crystals. This material is available free of charge via the Internet at <http://pubs.acs.org>.

REFERENCES

1. Cody, C. W., Prasher, D. C., Westler, W. M., Prendergast, F. G., and Ward, W. W. (1993) *Biochemistry* 32, 1212–1218.
2. Reid, B. G., and Flynn, G. C. (1997) *Biochemistry* 36, 6786–6791.
3. Nishiuchi, Y., Inui, T., Nishio, H., Bodi, J., Kimura, T., Tsuji, F. I., and Sakakibara, S. (1998) *Proc. Natl. Acad. Sci. U.S.A.* 95, 13549–13554.
4. Ormö, M., Cubitt, A. B., Kallio, K., Gross, L. A., Tsien, R. Y., and Remington, S. J. (1996) *Science* 273, 1392–1395.
5. Yang, F., Moss, L. G., and Phillips, G. N., Jr. (1996) *Nat. Biotechnol.* 14, 1246–1251.
6. Patterson, G. H., Knobel, S. M., Sharif, W. D., Kain, S. R., and Piston, D. W. (1997) *Biophys. J.* 73, 2782–2790.
7. Tsien, R. Y. (1998) *Annu. Rev. Biochem.* 67, 509–544.
8. Kneen, M., Farinas, J., Li, Y., and Verkman, A. S. (1998) *Biophys. J.* 74, 1591–1599.
9. Miyawaki, A., Llopis, J., Helm, R., McCaffery, J. M., Adams, J. A., Ikura, M., and Tsien, R. Y. (1997) *Nature* 388, 882–887.
10. Østergaard, H., Henriksen, A., Hansen, F. G., and Winther, J. R. (2001) *EMBO J.* 20, 5853–5862.
11. Chatteraj, M., King, B. A., Bublit, G. U., and Boxer, S. G. (1996) *Proc. Natl. Acad. Sci. U.S.A.* 93, 8362–8367.
12. Elsliger, M. A., Wachter, R. M., Hanson, G. T., Kallio, K., and Remington, S. J. (1999) *Biochemistry* 38, 5296–5301.
13. Bublit, G., King, B. A., and Boxer, S. G. (1998) *J. Am. Chem. Soc.* 120, 9370–9371.
14. Lakowicz, J. R. (1999) *Principles of Fluorescence Spectroscopy*, Kluwer Academic/Plenum, New York.
15. Albrecht, A. C., and Simpson, W. T. (1953) *J. Chem. Phys.* 21, 940.
16. Peterson, D. L., and Simpson, W. T. (1955) *J. Am. Chem. Soc.* 77, 3929–3930.
17. Peterson, D. L., and Simpson, W. T. (1957) *J. Am. Chem. Soc.* 79, 2375–2382.
18. Eaton, W. A., and Lewis, T. P. (1970) *J. Chem. Phys.* 53, 2164–2172.
19. Eaton, W. A., Hofrichter, J., Makinen, M. W., Andersen, R. D., and Ludwig, M. L. (1975) *Biochemistry* 14, 2146–2151.
20. Eaton, W. A. (1967) Doctoral Dissertation, The University of Pennsylvania, Philadelphia.
21. Eaton, W. A., and Hochstrasser, R. M. (1967) *J. Chem. Phys.* 46, 2533–2539.
22. Eaton, W. A., and Hochstrasser, R. M. (1968) *J. Chem. Phys.* 49, 985–995.
23. Churg, A. K., and Makinen, M. W. (1978) *J. Chem. Phys.* 68, 1913–1925.
24. Boxer, S. G., Kuki, A., Wright, K. A., Katz, B. A., and Xuong, N. H. (1982) *Proc. Natl. Acad. Sci. U.S.A.* 79, 1121–1125.
25. Metzler, C. M., Mitra, J., Metzler, D. E., Makinen, M. W., Hyde, C. C., Rogers, P. H., and Arnone, A. (1988) *J. Mol. Biol.* 203, 197–220.
26. Boxer, S. G., and Rosell, F. I. (2002), *Proceedings of the Biophysical Society, 46th Annual Meeting*, San Francisco, CA, The Biophysical Society, Bethesda, MD.
27. Inoué, S., Shimomura, O., Goda, M., Shribak, M., and Tran, P. T. (2002) *Proc. Natl. Acad. Sci. U.S.A.* 99, 4272–4277.
28. Lounis, B., Deich, J., Rosell, F. I., Boxer, S. G., and Moerner, W. E. (2001) *J. Phys. Chem. B* 105, 5048–5054.
29. Brejc, K., Sixma, T. K., Kitts, P. A., Kain, S. R., Tsien, R. Y., Ormö, M., and Remington, S. J. (1997) *Proc. Natl. Acad. Sci. U.S.A.* 94, 2306–2311.
30. Albrecht, A. C., and Simpson, W. T. (1955) *J. Chem. Phys.* 23, 1480–1485.
31. Kurimoto, M., Subramony, P., Gurney, R. W., Lovell, S., Chmielewski, J., and Kahr, B. (1999) *J. Am. Chem. Soc.* 121, 6952–6953.
32. Patterson, G. H., Piston, D. W., and Barisas, B. G. (2000) *Anal. Biochem.* 284, 438–440.

BI0266535